19th Brazilian Congress of Thermal Sciences and Engineering
November 6th–10th, 2022, Bento Gonçalves - RS - Brazil

ENC-2022-0092
ANALYTICAL MODEL OF MICROSSEGREGATION IN THE SOLIDIFICATION OF A BINARY ALLOY INCLUDING THERMODIFFUSION EFFECT

Romulo Heringer
Universidade Federal de Santa Catarina – UFSC, Campus Universitário, Trindade. 88040-900 – Florianópolis – SC
romulo.heringer@ufsc.br

Abstract. *This text presents a mathematical model for the microsegregation during the solidification of a binary alloy, considering thermodiffusion. Heat and solute mass transfer are evaluated in a dendrite branch by choosing the thermodynamic system in such a way that precludes chemical diffusion through its boundary, but the thermal gradient can drive thermodiffusion. The aim was to obtain a analytical equation for microsegregation where thermodiffusion parameters appear explicitly. With such a result, one can easily evaluate whether the phenomena inherent to the solidification process could enhance thermodiffusion when compared to solute transport without phase change. It seems that thermodiffusion coefficient should not be the better parameter to indicate the relevance of the Soret effect in the solidification process. Some dimensionless parameters emerge from the proposed model, which can be more suitable for this assessment.*

Keywords: *microsegregation modelling, Soret effect, thermodiffusion, solidification, heat and mass transfer*

1. INTRODUCTION

In the context of solidification, solute segregation means that the growing solid cannot dissolve the entire amount of components present in the solution, and the excess of chemical elements are rejected into the liquid in front of the solidification interface. As a result, the solid structure may present a non-uniform chemical distribution. Microsegregation stands to this phenomenon evaluated at scale of the smallest solidification structures. In the case of dendritic structures, this heterogeneity can be measured on the dendrite branches on the solidified material. On the other hand, the macrosegregation is the solute heterogeneity measured across the whole material, as a result of the transport of segregated species at the solid/liquid interface over longer distances compared to microstructures. This transport occurs by diffusion or convection trough the remaining liquid.

The Soret effect is the diffusion of chemical species in a mixture driven by thermal gradients. This kind of transport has been systematically neglected on solidification models (Dantzig and Rappaz (2009)). This simplification is based on the typically low values of the thermodiffusion coefficient in metallic solutions compared to the chemical driven diffusion coefficient. A parameter commonly used to show that is the Soret coefficient, S_T, defined by $S_T = D^T/D$, where D^T is the thermodiffusion coefficient, D is the diffusion coefficient. However, this parameter does not include other essential phenomena inherent to the solidification process, such as heat transfer, releasing of enthalpy of fusion, and solute segregation.

Recent results, such as those of references Satheesh and Mohan (2017) and Jafar-Salehi *et al.* (2016), suggest that in the cases studied, the thermodiffusion can influence relevant characteristics of solidified materials in a non-negligible manner. Accordingly, since the temperature gradient in the liquid is often high, the thermodiffusion may have a considerable influence on the composition of the liquid and the solidified final product. These results are perhaps associated with what has been noted by Platten and Legros, 1984 (Platten and Legros, 2012, p. 576): "The mass fraction gradient established under the effect of thermal diffusion is very small $(\cdots)$, but our theme is that such a small concentration gradient disproportionately influences hydrodynamics relative to its contribution to the buoyancy of the fluid. Therefore thermal diffusion cannot be ignored." Convection is not taken into account in the present model. However, microsegregation models are often coupled in multi-scale solidification modeling, where convection can be a significant player.

The present work is part of an effort to assess the influence of thermodiffusion in solidification processes. Initially, the objective is to obtain suitable parameters to evaluate the effect of thermodiffusion on the microsegregation scale. The

present work lies in this context. Subsequently, the Soret effect on macrosegregation shall be analyzed.

Several microsegregation models have been proposed. The Gulliver-Scheil microsegregation model (Kurz and Fisher (1998); Dantzig and Rappaz (2009)) is considered an effective tool for quantifying the solution concentration profile in the solidification process. Gulliver and later Scheil adopted a one-dimensional closed system defined so that this size is the half of secondary arm spacing, starting at the center of one of this arm. They could assume symmetry in the composition profiles at both boundaries. Several assumptions in the present work are similar to that of Gulliver and Scheil.

The scope of the present work is mainly the development of a microsegregation model, including the thermodiffusion effect, for which the heat and solute transport are evaluated. This is presented in section 2. In subsection 2.1 a physical model is established. Subsequently, in subsection 2.2 this physical model is translated to a mathematical description resulting in a boundary condition problem. An analytical solution is then proposed in subsection 2.3 The resulting equation, describing the solid fraction as a function of the temperature, exposes potential useful parameters for assessing the influence of thermodiffusion in solidification processes (subsection 2.4).

2. MICROSEGREGATION MODEL INCLUDING THERMODIFFUSION

2.1 Physical modeling

The present work concerns the dendritic solidification of a binary metallic alloy. We consider planar dendrite. In most cases, this implies a serious simplification, since we expect dendrites to be three-dimensional structures. However, there are also near planar growth. An example is a sample solidifying inside a thin crucible in an *in-situ* visualization experiment. The thermodynamic system adopted is a region between two secondary arms of an arbitrary planar dendrite. Like in the Gulliver-Scheil model, this region is defined in such a manner that it will result in a one-dimensional domain. Despite this, we will sometimes make reference to the volume (V) and the boundary area (S) of the system. Figure 1 shows our choice for the system. Above in the figure, light gray is a schematic representation of the halves of two neighboring dendrite secondary branches. The darker gray strip defines a region ($\delta y \times \lambda_2 \times 1$) distant enough from both, tip and base of the branches so that the two solid-liquid interfaces are near planar. λ_2 is the secondary arm spacing, an important parameter in dendrite growth (Flemings (1974); Kurz and Fisher (1998); Dantzig and Rappaz (2009)). Considering x an axis orthogonal to the longitudinal direction of the branch crossing the position Y, we take $x = 0$ at the center of the left branch, as shown in the schematic graph below in the figure 1. $x = \mathcal{X}$ is the position for which $dC/dx = 0$ so that chemical diffusion is precluded there, even in the case where temperature differences between two neighbor branches would be measurable. A common but often unnecessary simplification is to do $\mathcal{X} = \lambda_2/2$. Besides, if L is the branch length, we choose $\delta y \ll L$. This proposition allows us to neglect any variation on y direction, resulting in a one-dimensional analysis along x. From the above discussion, in the present work the thermodynamic system consists of a volume $\mathsf{V} = \delta y \times \mathcal{X} \times 1$, initially fully liquid. However, taking $\partial C/\partial y = 0$ for $Y \leq y \leq (Y + \delta y)$, our mathematical domain reduces to the one-dimensional interval $0 \leq x \leq \mathcal{X}$. The solidification starts from $x = 0$ and develops toward $x = \mathcal{X}$, when the volume is fully solid. During solidification, at any time t there is a planar solid-liquid interface at $x = x^*$. There is no diffusion driven by chemical gradients trough the system boundaries, because $\partial C/\partial y = 0$ and $(dC/dx)_{\mathcal{X}} = 0$.

In order to proceed, additional considerations are necessary for transport phenomena and the concerned physical properties. For metallic alloys, it is common that $D_\ell \gg D_s$, where D_ℓ and D_s are the liquid and the solid solute diffusion coefficient, respectively. This has been used by Gulliver and by Scheil to neglect the diffusion in the solid phase (back diffusion) in their microsegregation model (Dantzig and Rappaz (2009)). In the present work, we shall also assume there is no back diffusion. This is a good approach when the solidification time (t_f) is less than $10^3\mathtt{s}$ (Dantzig and Rappaz, 2009, p. 397). This fact takes us to our next simplification.

Our system length is $\mathcal{X} \sim \lambda_2/2$ (figure 1). On the other hand, λ_2 evolves proportionally to square root of time (Kurz and Fisher, 1998, p. 85, 259). Fewer solidification time implies smaller $\mathcal{X}$. For example, measurements for a wide range of solidification conditions of Al-4.5wt%Cu, shows that $5\ \mu\mathtt{m} < \lambda_2 < 10^3\ \mu\mathtt{m}$ (Kurz and Fisher, 1998, p. 87). For $t_f = 10^3\ \mathtt{s}$, the upper limit for the present model, these data show that $\lambda_2 \sim 10^2\ \mu\mathtt{m}$. For such a small region, we can consider diffusion in the liquid fast enough to establish a uniform solute profile in this phase.

We shall also consider local thermodynamic equilibrium at the solid-liquid interface. That is, the equilibrium phase diagram can be directly used to describe solute segregation and the thermodynamic coordinates (temperature and solute fraction) on the solid-liquid interface. Moreover, one can later introduce the effects of possible non-equilibrium solidification, such that solute trapping in rapid solidification, using an appropriate correction for the partition coefficient Aziz (1982). The densities of the solid and the liquid phases are considered equal and constant during solidification. Thus, we do not take into account the solidification shrinkage or any other source of phase movement.

Finally, to include the thermodiffusion effect, we argue that solute can diffuses across the system boundaries driven by thermal gradients. However, we assume that this transport can only be done through the liquid phase. Withal, we consider thermodiffusion between the system and its neighborhood but not inside the system, where the thermal gradient is negligible due to its typical size.

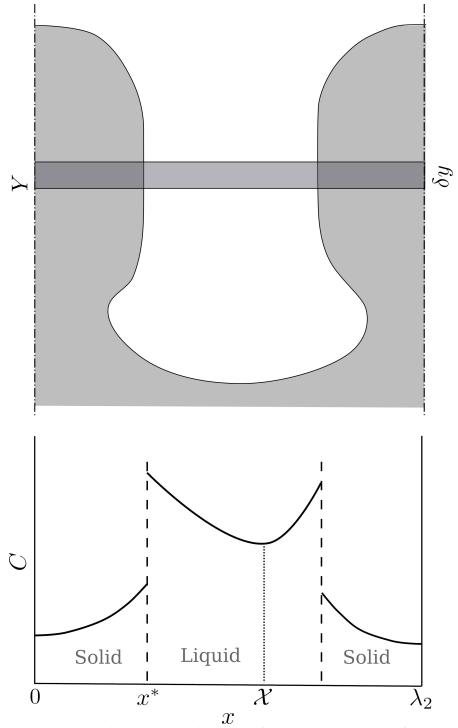

Figure 1: Locus of the thermodynamic system. Above: schematic representation of the halves of two neighboring dendrite secondary branches (light gray); definition of a region ($\delta y \times \lambda_2 \times 1$), distant enough from both, tip and base of the branches (darker gray). Below: schematic solute profiles along an x axis transversal to the branches represented above, at the position Y. $x = \mathcal{X}$ is the position for which $dC/dx = 0$.

Table 1 summarizes the main hypotheses and assumptions presented above. Two additional simplifications will be introduced later in the text. Hypotheses H1 to H8 are similar to those established by Gulliver and Scheil Kurz and Fisher (1998); Dantzig and Rappaz (2009). Different from them, the inclusion of H9 makes the present system a control volume (an open system).

Table 1: Hypotheses for the present model.

Assumption		**Modeling concerns**
H1	$\frac{\partial C}{\partial y} = 0$ for $Y \leq y \leq (Y + \delta y)$	One-dimensional domain $0 \leq x \leq \mathcal{X}$.
H2	$\delta y \ll \mathcal{X} \sim \frac{\lambda_2}{2}$	The solid-liquid interface is locally flat and its position over time is $x^*(t)$, with $0 \leq x^*(t) \leq \mathcal{X}$.
H3	$\left(\frac{dC}{dx}\right)_{\mathcal{X}} = 0$	There is no solute diffusion across the boundaries due to chemical gradientes.
H4	Local equilibrium	(T^*, C^*) from *liquidus* and *solidus* lines.
H5	$\mathcal{X} \propto t_f{}^{\frac{1}{3}}$	Solute profile uniform on the liquid phase. In conjunction with H5, this means that $C_\ell = C_\ell^*$ everywhere in the liquid. C_ℓ^* is the *liquidus* solute fraction at the given temperature.
H6	Liquid and solid densities are equal and constant	No solidification shrinkage.
H7	Liquid is static	No convection.
H8	Thermodiffusion	Solute flows trough the boundaries due to thermal gradients.
H9	Position $\mathcal{X}$ remains constant	If $\mathcal{X}$ is constant, the volume of the system is constant too ($\mathsf{V} = \delta y \times \mathcal{X} \times 1$).
H10	$D_\ell \gg D_s$	No solute diffusion in the solid phase.

2.2 Mathematical modeling

The order of λ_2 is about $10^{-6}\,\mathtt{m}$. The total amount of solute in a control volume defined in accordance to the constraints H1, H2, H6 and H8 (table 1) may be expressed as follows

$$\int_0^{x^*(t)} C_{\mathtt{B}s}(x,t)dx + \int_{x^*(t)}^{\mathcal{X}(t)} C_{\mathtt{B}\ell}(x,t)\,dx = \mathcal{X}(t)\bar{C}_{\mathtt{B}}(t) \tag{1}$$

In the present text, $C_{\mathtt{B}} \equiv \rho_{\mathtt{B}}/\rho$ is the mass fraction of specie B on a single phase; $\rho_{\mathtt{B}}$ is the mass density of specie B and ρ is the mass density of the mixture, a binary alloy (A-B) in the present work. The subscript "ℓ" refers to the liquid phase, while "s" indicates the solid phase. $\bar{C}_{\mathtt{B}}$ is the solute mass fraction averaged over the entire (liquid plus solid) control volume $0 \leq x \leq \mathcal{X}(t)$. We consider that $\bar{C}_{\mathtt{B}}$ may vary over time. The integration limit x^* is the location of the solid-liquid interface. For convenience, we will omit the subscript B where only the solute is concerned.

According to hypothesis H5, the solute composition is considered uniform in the liquid region and it is equal to the liquid composition on the solidification interface, C_ℓ^*, resulting in

$$\int_0^{x^*} C_s\,dx \;+\; (\mathcal{X} - x^*)\,C_\ell^* \;= \mathcal{X}\,\bar{C} \tag{2}$$

For simplicity, the (x,t) function notation have been omitted. Hereafter also $(\mathcal{X} - x^*) = x_\ell^*$. Dividing Eq. (2) by $\mathcal{X}$ and defining the volumetric liquid fraction, $g_\ell \equiv \mathsf{V}_\ell/\mathsf{V} = x_\ell^*/\mathcal{X}$. Doing this and differentiating the resulting equation with respect to time, we have

$$-\left(\frac{1}{\mathcal{X}}\right)^2\left(\int_0^{x^*} C_s\,dx\right)\frac{d\mathcal{X}}{dt} \;+\; C_s^*\,\frac{dg_s}{dt} \;+\; \int_0^{g_s}\frac{\partial C_s}{\partial t}\,dg_s \;+\; g_\ell\,\frac{dC_\ell^*}{dt} \;+\; C_\ell^*\,\frac{dg_\ell}{dt} \;=\; \dot{\bar{C}} \tag{3}$$

where was also defined the volumetric solid fraction $g_s \equiv (\mathsf{V}_s/\mathsf{V}) = x^*\,(1/\mathcal{X})_t$, so that $(1/\mathcal{X})_t\,dx = dg_s$, with $\mathsf{V}_\ell + \mathsf{V}_s = \mathsf{V}$, so $dg_s = -dg_\ell$. The subscript t indicates an instantaneous value at time t and $C_s^* = C_s(x^*,t)$. In addition, it was made $\dot{\bar{C}} \equiv d\bar{C}/dt$.

From the equilibrium phase diagram (hypothesis H4) is defined the partition coefficient: $k_0 \equiv C_s^*/C_\ell^*$. So, $C_s^*\,(dg_s/dt) = -k_0\,C_\ell^*\,(dg_\ell/dt)$. Also, $\mathcal{X}$ does not depend on x, allowing to do $dx/\mathcal{X} = d(x/\mathcal{X}) = d(\mathsf{V}_s/\mathsf{V}) = dg_s$ for $0 \leq x \leq x^*$, in the first integral of Eq. (3). Equation (3) becomes,

$$\frac{1}{\mathcal{X}}\,\frac{d\mathcal{X}}{dt}\;\int_0^{(1-g_\ell)} C_s\,dg_\ell \;-\int_0^{(1-g_\ell)}\frac{\partial C_s}{\partial t}\,dg_\ell \;+ g_\ell\,\frac{dC_\ell^*}{dt} \;+ (1-k_0)\,C_\ell^*\,\frac{dg_\ell}{dt} \;=\dot{\bar{C}} \tag{4}$$

Equation (4) quantifies the evolution of solute content in a system subjected to the assumptions H1 to H7. If $\dot{\bar{C}} \neq 0$, the system is open and, in absence of convection, the hypothesis H8 states that solute flows through the system boundary by thermodiffusion.

Until this point we did not use hypotheses H9 and H10. In fact, Eq. (4) is suitable where diffusion in the solid cannot be ignored. Also, the first term of Eq. (4) take into account the variations of the parameter $\mathcal{X}$ (e. g. related to the evolution of secondary arm spacing). For our model, $d\mathsf{V} = d\mathcal{X}$ (H1).

However, in the present work we deal with a simplified version of Eq. (4), by applying H9 ($\mathcal{X}$ is constant) and H10 (no back diffusion) to get

$$g_\ell\,\frac{dC_\ell^*}{dt} + (1-k_0)\,C_\ell^*\,\frac{dg_\ell}{dt} \;=\dot{\bar{C}} \tag{5}$$

To proceed, we must evaluate $\dot{\bar{C}}$ by assessing the solute flow through the boundary system. For a system with volume V and boundary surface S, without chemical reaction, the mass balance of a solute B in a mixture is

$$\frac{d}{dt}\int_{\mathsf{V}} \rho_{\mathtt{B}}\,d\mathsf{V} = -\int_{\mathsf{S}} \vec{j}_{\mathtt{B}}\cdot\hat{n}\,d\mathsf{S} \tag{6}$$

where $\rho_{\mathtt{B}} \equiv m_{\mathtt{B}}/\mathsf{V}$, with $m_{\mathtt{B}}$ being the mass of solute in V; $\vec{j}_{\mathtt{B}}$ is the flux of B such that $[\vec{j}_{\mathtt{B}}] = \mathtt{kg\,m^{-2}\,s^{-1}}$.

Dividing Eq. (6) by the total mass of the system, $\rho\,\mathsf{V}$, and applying assumption H5 (ρ constant and uniform in V), we have

$$\frac{1}{\mathsf{V}}\,\frac{d}{dt}\int_{\mathsf{V}} C_{\mathtt{B}}\,d\mathsf{V} = -\frac{1}{\rho\,\mathsf{V}}\int_{\mathsf{S}} \vec{j}_{\mathtt{B}}\cdot\hat{n}\,d\mathsf{S} \tag{7}$$

V is considered constant over time (hypothesis H9) and $1/\mathsf{V}$ can enter the time derivative. Then, the left side of Eq. (7) is then recognized as $\dot{\bar{C}}$.

Also, using the hypotheses H3 and H8, we have that $\vec{j} = \vec{j}^T$, the vector of solute flux by thermodiffusion, which can be noted as (De Groot and Mazur, 2013, p. 275),

$$\vec{j}^T = -\frac{L_{\mathtt{B}q}}{T^2}\,\vec{\nabla} T \tag{8}$$

$L_{\mathtt{B}q}$ is the Onsager's phenomenological coefficient related to thermodiffusion of solute $\mathtt{B}$. $L_{\mathtt{B}q}$ is not readily available, but can be written in terms of a thermodiffusion coefficient, D^T, whose dimension in the International System of Units is $[D^T] = \mathtt{m}^2\,\mathtt{s}^{-1}\,\mathtt{K}^{-1}$. D^T is done by (De Groot and Mazur, 2013, p. 276)

$$L_{\mathtt{B}q} = \rho\, C_{\mathtt{A}}\, C_{\mathtt{B}}\, D^T\, T^2 \tag{9}$$

$C_{\mathtt{A}}$ is the solvent mass fraction, so that $C_{\mathtt{A}}\, C_{\mathtt{B}} = C_{\mathtt{B}}\,(1 - C_{\mathtt{B}})$. Equation (9) will be useful later in this work. However, for now we maintain Eq. (8) to take $\vec{j}^T$ into Eq. (7), to get

$$\dot{\bar{C}} = \frac{1}{\rho\,\mathsf{V}}\,\frac{L_{\mathtt{B}q}}{T^2}\int_{\mathsf{S}} \vec{\nabla} T\cdot\hat{n}\,d\mathsf{S} \tag{10}$$

where we consider $L_{\mathtt{B}q}$ and T uniform over S.

To evaluate the surface integral on (7) we shall take a heat balance over V. Hypothesis H7 restricts heat transfer to conduction alone so that thermal balance over the constant V is

$$\rho\, c\int_{\mathsf{V}} \frac{\partial T}{\partial t}\,d\mathsf{V} = -\int_{\mathsf{S}} \vec{q}\cdot\hat{n}\,d\mathsf{S} + \int_{\mathsf{V}} \frac{dg_s}{dt}\,L_f\,d\mathsf{V} \tag{11}$$

L_f is the enthalpy of fusion with $[L_f] = \mathtt{J}\,\mathtt{m}^{-3}$. Applying Fourier's law for the heat flux and the hypotheses of table 1 allowing consider uniform fields over V, done

$$\int_{\mathsf{S}} \vec{\nabla} T\cdot\hat{n}\,d\mathsf{S} = \frac{\rho\, c}{\bar{\kappa}}\,\mathsf{V}\,\frac{dT}{dt} + \frac{L_f}{\bar{\kappa}}\,\mathsf{V}\,\frac{dg_\ell}{dt} \tag{12}$$

where we have used $dg_s/dt = -dg_\ell/dt$. The property $\bar{\kappa}$ is a convenient average of the thermal conductivity κ over the entire surface S. If the thermodiffusion is believed occurs mainly through liquid surface, then $\bar{\kappa} \to \kappa_\ell$. In the present text the $\bar{\kappa}$ notation is kept.

Using the result (12) in Eq. (10), and then in (5) done

$$g_\ell\,\frac{dC_\ell^*}{dt} + (1-k_0)\,C_\ell^*\,\frac{dg_\ell}{dt} = \frac{c\,L_{\mathtt{B}q}}{\bar{\kappa}}\,\frac{1}{T^2}\,\frac{dT}{dt} + \frac{L_{\mathtt{B}q}\,L_f}{\rho\,\bar{\kappa}}\,\frac{1}{T^2}\,\frac{dg_\ell}{dt} \tag{13}$$

Assuming that the *liquidus* curve can be approximated locally by a straight line with a slope m_ℓ, we obtain $T - T_f = m_\ell\, C_\ell^*$ and $dC_\ell^*/dt = (1/m_\ell)\,dT/dt$. T_f is the melting temperature of the pure solvent. Using this approach in Eq. (13) and re-arranging done

$$(k_0-1)\left[T^2\,(T-T_f) + \frac{m_\ell\,L_{\mathtt{B}q}\,L_f}{(k_0-1)\rho\,\bar{\kappa}}\right]\frac{dg_\ell}{dt} = \left(-\frac{m_\ell\,c\,L_{\mathtt{B}q}}{\bar{\kappa}} + T^2\,g_\ell\right)\frac{dT}{dt} \tag{14}$$

Taking an aluminum alloy as reference (table 2), we can evaluate the order of each term of Eq. (14):

$$(k_0-1)\,T^2\,(T-T_f) \sim 10^4; \quad \frac{m_\ell\,L_{\mathtt{B}q}\,L_f}{\rho\,\bar{\kappa}} \sim 10^2; \quad \frac{m_\ell\,c\,L_{\mathtt{B}q}}{\bar{\kappa}} \sim 10^0; \quad T^2\,g_\ell \sim 10^3$$

Based on the above statements we will neglect the first term on the right side of Eq. (14), that is, the contribution of thermal inertia [1]. For the cases where this holds, the differential Eq. (14) becomes separable, and the resulting boundary value problem is as follows.

$$(k_0-1)\,\frac{1}{g_\ell}\,dg_\ell = \frac{T^2}{T^2\,(T-T_f)+E}\,dT \tag{15}$$

with the boundary conditions

$$g_\ell(T) = 1 \quad \text{at} \quad T = T_0 \tag{16}$$

where T_0 is the *liquidus* temperature related to the nominal solute fraction. Physically, we are restricted to $T \in [T_e, T_f)$; T_e is the eutectic temperature. To simplify writing, it was defined E, considered a constant:

$$E = \frac{m_\ell\,L_{\mathtt{B}q}\,L_f}{(k_0-1)\,\rho\,\bar{\kappa}} \tag{17}$$

[1] A derivation from the present approach has been presented in Santos Filho and Heringer (2020), where thermal inertia is taken into account, but not the latent heat. This is made by evaluating the thermal gradient at the boundary of the liquid phase only.

2.3 Resolution of the boundary value problem

Our goal in this section is to solve the the differential subject to the boundary condition, summarized at Eqs. (15) and (16). Taking $f(T)$ as the integrand at right side of Eq. (15), we can verify that, for $0 < T < T_f$,

$$f(T) = \frac{T^2}{T^2\,(T - T_f) + E} = \sum_{n=1}^{\infty} \left[(-1)^{n-1} \frac{E^{n-1}}{T^{2(n-1)}\,(T - T_f)^n} \right] \tag{18}$$

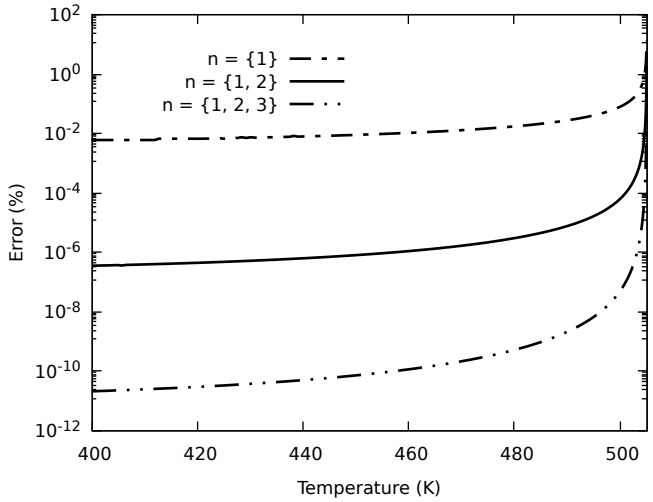

Figure 2: Percentage error when taking 1, 2 and 3 summation terms compared to $f(T)$. In these results were used $E = 10^3\,\mathtt{K}^3$, $T_f = 500\,\mathtt{K}$. The approximation fails for $T \sim T_f$.

Figure 2 shows the deviation between $f(T)$ and the results of the summation proposed in Eq. (18), taking 1, 2 and 3 terms. E and T_f values are indicated at the figure caption. These results show that we can safely consider the first and the second terms of the sum, neglecting the rest. Even for $|T - T_f| \sim 1\,\mathtt{K}$ (low solute concentrations) the error is around $2 \cdot 10^{-3}\,\%$ (figure 2, red curve). However, Eq. (18) clearly fails for T too close to T_f, i. g. $0 < |T - T_f| < 1\,\mathtt{K}$. Other values for E and T_f have also been used with similar conclusions. Then, the approximation proposed is

$$f(T) \approx \frac{1}{T - T_f} - \frac{E}{T^2\,(T - T_f)^2} \tag{19}$$

Equations (15), (18) and (19) lead to the following differential equation

$$(k_0 - 1)\,\frac{1}{g_\ell}\,dg_\ell = \left[\frac{1}{T - T_f} - \frac{E}{T^2\,(T - T_f)^2} \right] dT \tag{20}$$

Integrating both sides of Eq. (20) considering the limits from the boundary conditions (16) done

$$g_\ell \;=\; \left(\frac{T - T_f}{T_0 - T_f} \right)^{\frac{1 + 2E/T_f^3}{k_0 - 1}} \left(\frac{T}{T_0} \right)^{\frac{-2E/T_f^3}{k_0 - 1}} \exp\left\{ \frac{2\,E}{(k_0 - 1)\,T_f^2} \left[\frac{2\,T - T_f}{T\,(T - T_f)} - \frac{2\,T_0 - T_f}{T_0\,(T_0 - T_f)} \right] \right\} \tag{21}$$

Finally, the solid fraction g_s considering thermodiffusion effect is then

$$g_s \;=\; 1 - \left(\frac{T - T_f}{T_0 - T_f} \right)^{\frac{1 + 2E/T_f^3}{k_0 - 1}} \left(\frac{T}{T_0} \right)^{\frac{-2E/T_f^3}{k_0 - 1}} \exp\left\{ \frac{2\,E}{(k_0 - 1)\,T_f^2} \left[\frac{2\,T - T_f}{T\,(T - T_f)} - \frac{2\,T_0 - T_f}{T_0\,(T_0 - T_f)} \right] \right\} \tag{22}$$

It can be noted that, if $E = 0$, Eq. (22) equals the Gulliver-Scheil solution for microsegregation.

2.4 Dimensionless parameters

From the exponents of equations (22) or (21) we recognize that

$$\frac{E}{T_f^3} = \frac{m_\ell\,L_{\mathtt{B}q}\,L_f}{(k_0 - 1)\,\rho\,\bar{\kappa}}\,\frac{1}{T_f^3} = \frac{m_\ell\,C_{\mathtt{A}0}\,C_{\mathtt{B}0}\,D^T\,T_0^2\,L_f}{(k_0 - 1)\,\bar{\kappa}\,T_f^3} \tag{23}$$

where Eq. (9), evaluated at T_0, have been used (the pair $(C_{\{\mathtt{A,B}\}0}, T_0)$ is a point on the *liquidus* line). The term $(\rho\, C_{\mathtt{A}0}\, C_{\mathtt{B}0}\, D^T)$ is a coefficient for thermodiffusion. We can group the parameters appearing in Eq. (23) in different ways, as follows.

$$\mathsf{H}_1 = \frac{m_\ell}{T_f\,(k_0-1)};\quad \mathsf{H}_2 = \frac{D^T\,L_f}{\bar{\kappa}};\quad \mathsf{H}_3 = \frac{m_\ell}{T_f\,(k_0-1)}\,\frac{D^T\,L_f}{\bar{\kappa}};\quad \mathsf{H}_4 = \frac{m_\ell}{T_f\,(k_0-1)}\,C_{\mathtt{A}0}\,C_{\mathtt{B}0}\,\frac{D^T\,L_f}{\bar{\kappa}}\left(\frac{T_0}{T_f}\right)^2 \tag{24}$$

The dimensionless term H_1 quantifies the solute segregation strength. More segregation implies more solute available to diffuse through the liquid. On the other hand, in $L_f/\bar{\kappa}$ the amount of enthalpy liberated due to solidification (pointed by L_f) is rated to how easy the heat is driven away by conduction (quantified by $\bar{\kappa}$). Higher $L_f/\bar{\kappa}$ indicates greater temperature gradient, leading to more thermodiffusion. In this way, H_2 could represent the influence of the heat transfer with phase change on thermodiffusion. The specific heat is absent because the effect of thermal inertia has been neglected. H_2 does not include the influence of solute segregation on thermodiffusion. To do so, it should be considered at least the parameter $\mathsf{H}_3 = \mathsf{H}_1\,\mathsf{H}_2$ or H_4. We could also include in H_4 (the last of Eqs. (24)) the term $(k_0-1)^{-1}$ from the exponents in (22) or (21), resulting this quantity appearing squared in the denominator of a whole dimensionless parameter, H, defined as follows.

$$\mathsf{H} = -\frac{m_\ell\,L_{\mathtt{B}q}\,L_f}{(k_0-1)^2\,\rho\,\bar{\kappa}\,T_f^3} = -\frac{m_\ell}{T_f\,(k_0-1)^2}\,C_{\mathtt{A}0}\,C_{\mathtt{B}0}\,\frac{D^T\,L_f}{\bar{\kappa}}\left(\frac{T_0}{T_f}\right)^2 \tag{25}$$

By including a minus signal in the right side of Eq. (25), we force H to take the signal of D^T (for $m_\ell < 0$). H seems to be suitable for evaluating the thermodiffusion effect during the solidification of a binary alloy. However, grouping the quantities in Eqs. (24) in another way could result in a parameter with more appropriate physical meaning. That is not the scope of the present work. For now, applying the definition (25) in Eq. (22), we have finally

$$g_s = 1 - \left(\frac{T-T_f}{T_0-T_f}\right)^{\left(\frac{1}{k_0-1}-2\mathsf{H}\right)}\left(\frac{T}{T_0}\right)^{2\mathsf{H}}\exp\left\{-2\mathsf{H}\,T_f\left[\frac{2\,T-T_f}{T\,(T-T_f)} - \frac{2\,T_0-T_f}{T_0\,(T_0-T_f)}\right]\right\} \tag{26}$$

Equation (26) is the final result of the present microsegregation model including Soret effect. According to Eq. (26), the influence of thermodiffusion on solidification path is affected by both, the solute segregation and the amount of enthalpy of fusion liberated in the process. Thermal inertia proved to be negligible in this mechanism compared to both segregation and latent heat.

3. RESULTS AND DISCUSSIONS

In this section, we compare the results from the present model with those without the thermodiffusion effect (Gulliver-Scheil equation). The aim is to assess the conditions for which thermodiffusion becomes non-negligible in the context of microsegregation.

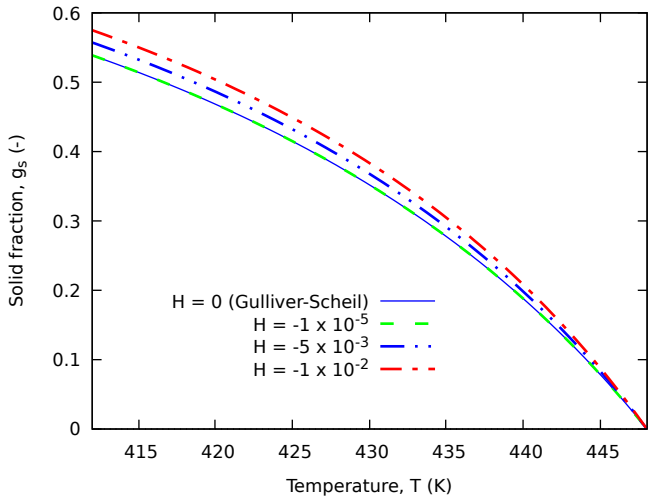

Figure 3: Solidification paths for an pseudo-alloy based on Sn-Bi system, calculated using Gulliver-Scheil equation and the present model for arbitrary values of parameter H.

Figure 3 shows solidification paths calculated from Eq. (26). These results were obtained using properties of an Sn-Bi alloy (summarized at table 2) except for the parameter H, which values were artificially imposed from $\mathsf{H} = 0$ (Gulliver-Scheil) to $\mathsf{H} = 10^{-2}$.

The sign of H cause the curve of solid fraction versus temperature be above ($\mathsf{H} < 0$) or below ($\mathsf{H} > 0$) of the path calculated using Gulliver-Scheil equation. The strength of Soret effect is quantified by $|\mathsf{H}|$, the absolute value of H. Figure 4 shows the percentage difference between the solidification path calculated using the indicated H and that using $\mathsf{H} = 0$ (no thermodiffusion). That means, $\%\,\text{Difference} = 100\,(|g_s - g_{s,\mathsf{H}=0}|)/(g_{s,\mathsf{H}=0})$. The physical parameters used in these results are from the phase diagrams of Sn-Bi and Al-Cu alloys. It can be noted that, for these cases, the difference is around $1\,\%$ for $|\mathsf{H}| \sim 10^{-3}$ and increases for higher values of $|\mathsf{H}|$. These results suggest that H is an important parameter to decide whenever thermodiffusion is non-negligible for the microsegregation of binary alloys.

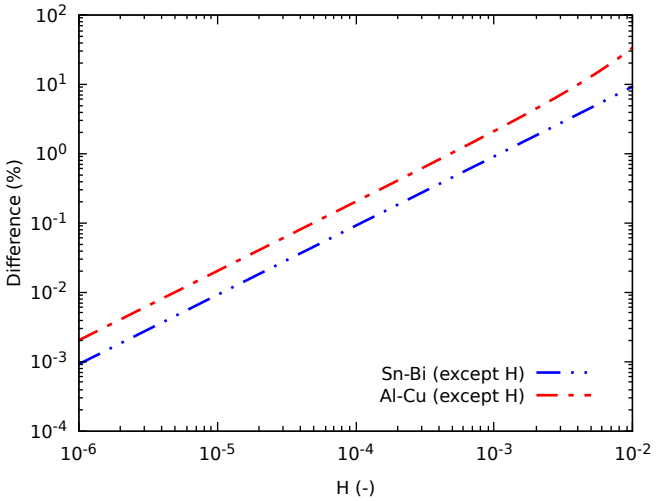

Figure 4: Evaluation of H influence using the percentage difference between the solidification paths calculated from Eq. (26) and from Gulliver-Scheil equation. The curves were produced using Sn-Bi (lower curve) and Al-Cu (upper curve) phase diagrams, except for the imposed parameter H.

The arbitrary values of H in the figures 3 and 4 makes those conditions pseudo-alloys. Figure 5 shows results for real alloys. The main graph at the top of figure 5 is the solidification path of Sn-35wt%Bi, from T_0 to the eutectic temperature ($412\,\mathtt{K}$). The smaller graph is a magnification of the same curve near the eutectic temperature. The graph at the bottom of figure 5 shows the percentage difference between g_s calculated using (26) with real H and g_s calculated for Sn-35wt%Bi with $\mathsf{H} = 0$ (Gulliver-Scheil).

Table 2: Physical properties and calculation conditions.

Property	**Value [Reference]**	
	Sn-Bi	**Al-Cu**
Nominal solute fraction, C_0 [wt%]	35.0	4.5
Initial *liquidus* temperature, T_0 [K]	448.0	918.4
Melting point, T_f [K]	505.11 [Vizdal *et al.* (2007)]	933.6 [Aksöz *et al.* (2010)]
Liquidus slope, m_ℓ [$\mathtt{K}\,(\text{wt\%})^{-1}$]	-1.6314	-3.37
Partition coefficient, k_0 [-]	0.368	0.17
Thermal conductivity [a], κ_ℓ [$\mathtt{J\,m^{-1}\,s^{-1}\,K^{-1}}$]	25 [Giordanengo *et al.* (1999)]	140 [Giordanengo *et al.* (1999)]
Enthalpy of fusion, L_f [$\mathtt{J\,m^{-3}}$]	$4.3 \cdot 10^8$ [Chen *et al.* (1998)]	$8.43 \cdot 10^8$ [Aksöz *et al.* (2010)] [c]
Thermodiffusion coefficient, D^T [$\mathtt{m^2\,s^{-1}\,K^{-1}}$]	$-1.67 \cdot 10^{-11}$ [Eslamian *et al.* (2010)] [b]	$6.21 \cdot 10^{-12}$ [Bhat (1975)]
Density, ρ [$\mathtt{kg\,m^{-3}}$]	$8.7 \cdot 10^3$ [Dobosz and Gancarz (2018)]	$2.4 \cdot 10^3$ [Plevachuk *et al.* (2008)]

[a] It was considered $\bar{\kappa} = \kappa_\ell$.

[b] D^T was evaluated from the thermodiffusion factor $\alpha_T = D^T\,T_0/D$, with $\alpha_T = -0.396$ for Sn-Bi (Eslamian *et al.* (2010)); D is the chemical diffusion coefficient ($D = 1.89 \cdot 10^{-9}\,\mathtt{m^2\,s^{-1}}$).

[c] Averaged between values for Al-3wt%Cu and for Al-6wt%Cu.

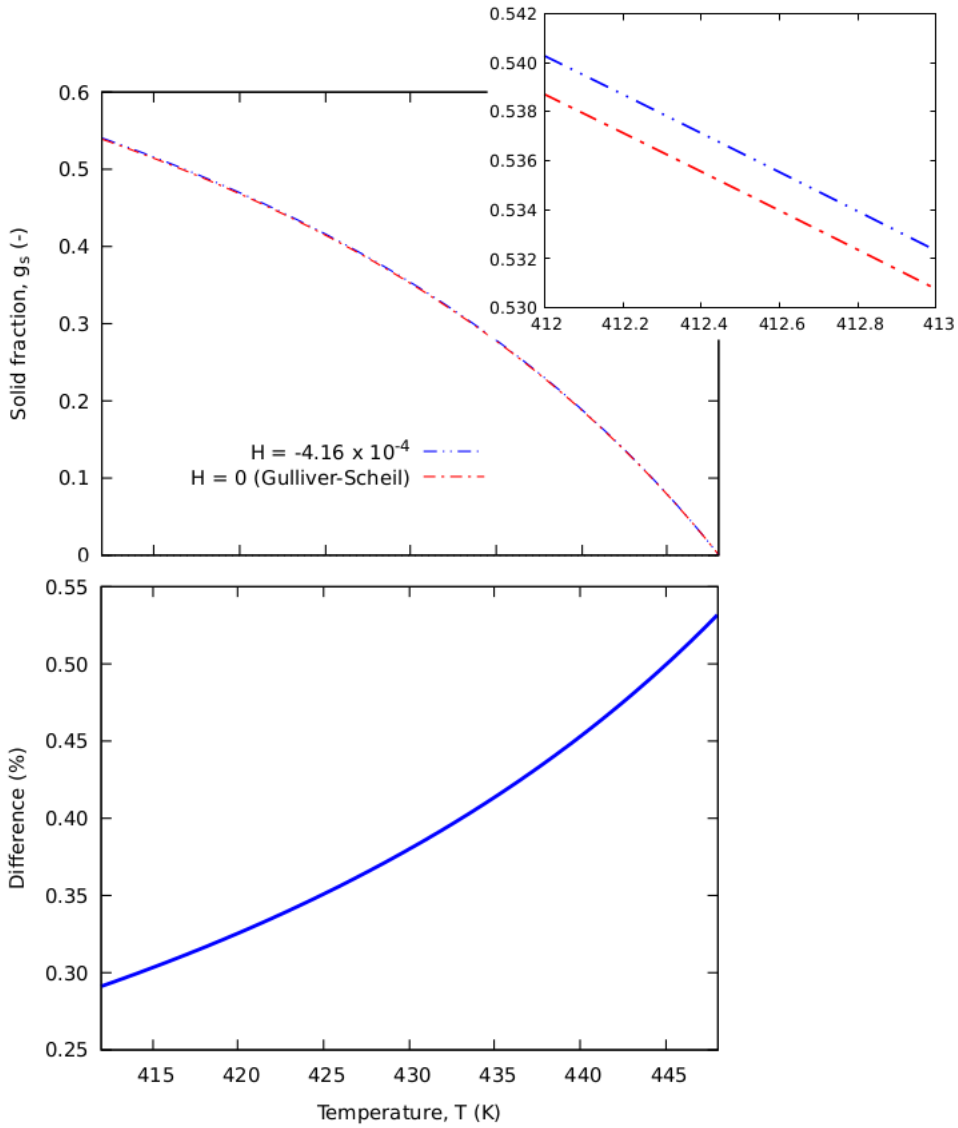

Figure 5: Top – Solidification paths for an Sn-35.0wt%Bi alloy calculated using Gulliver-Scheil equation ($\mathsf{H} = 0$) and the present model; the overlapping graph is an enlargement close to the eutectic temperature. Bottom – Percentage difference between the solidification paths calculated using Gulliver-Scheil equation and the present model, for Sn-35.0wt%Bi alloy.

Taking into account the data from table 2 considering the Sn-35wt%Bi, we find $\mathsf{H} \approx -4.16 \cdot 10^{-4}$. Therefore, for this alloy, according to figure 3 (bottom), we can wait an effect of thermodiffusion on g_s around $10^{-1}\,\%$, compared to the case disregarding thermodiffusion. Actually, the graph at the bottom of figure 5 shows this percentage difference along the solidification path of Sn-35wt%Bi. The variation is from $\sim 0.53\,\%$ at the beginning of solidification to $\sim 0.29\,\%$ at the eutectic temperature. In conclusion, for this case, the Soret effect on the evolution of the solid fraction seems to be no significant. However, this does not mean this effect can not be relevant for other phenomena during solidification (about this, consider the statement of (Platten and Legros, 2012, p. 576) (see verbatim on page 1).

For the Al-4.5wt%Cu we have $\mathsf{H} \approx 8.15 \cdot 10^{-5}$. The percentage difference variation is from $\sim 0.85\,\%$ at the beginning of solidification to $\sim 0.9\,\%$ at the eutectic temperature. It should be note that the average percentage difference is smaller for Al-4.5wt%Cu than for Sn-35wt%Bi. This is coherent with the fact that $|\mathsf{H}_{\mathrm{Sn35wt\%Bi}}| > |\mathsf{H}_{\mathrm{Al4.5wt\%Cu}}|$. The precedent inequality seems mainly influenced by $\left|D^T_{\mathrm{Sn35wt\%Bi}}\right| > \left|D^T_{\mathrm{Al4.5wt\%Cu}}\right|$. However, this is not straightforward considering all other parameters concerned: (L_f/κ), $(m_\ell/T_f\,(k_0 - 1))$. More alloys shall be evaluated to verify if H (or H_3) is a better parameter than D^T in the assessment of thermodiffusion effect on solidification process.

4. CONCLUSIONS

In this work, we have presented the analytical development of a microsegregation model that includes the thermodiffusion effect. This model applies to binary alloys solidification. A thermal balance allows assessing the temperature

gradient on the system boundary, the driving force for thermodiffusion. The term of thermal inertia was neglected face to enthalpy releasing and segregation contributions.

A set of dimensionless parameters emerges naturally from the model, which correlates thermodiffusion, heat transfer, and the amount of solute segregated due to solidification. In single-phase transport, D^T is enough to evaluate the thermodiffusion effect. Nevertheless, in solidification processes, in addition to the thermodiffusion coefficient itself, the solute content, the *liquidus* slope, the partition coefficient, and the enthalpy of fusion influence the thermodiffusion relevance in solidification phenomena.

Depending on the value of $|\mathsf{H}|$, we can attempt a non-negligible difference between the solidification paths calculated using the present model and those without thermodiffusion (Gulliver-Scheil equation). The present model was applied to calculate the solidification path of Sn-35wt%Bi and Al-4.5wt%Cu alloys, for which $|\mathsf{H}| \approx 4.16 \cdot 10^{-4}$ and $|\mathsf{H}| \approx 8.15 \cdot 10^{-5}$, respectively. The results have shown no significant relevance of the thermodiffusion effect on solid fraction path in these cases. Keeping other conditions from table 2 and varying H, it was found that $|\mathsf{H}| \sim 10^{-3}$ causes a percentage difference of the order of $1\,\%$. This difference increases for higher values of $|\mathsf{H}|$.

More studies are necessary to verify the usefulness of H and $\mathsf{H}_{\{1,2,3\}}$ as similarity parameters.

5. REFERENCES

Aksöz, S., Ocak, Y., Maraşlı, N., Çadirli, E., Kaya, H. and Böyük, U., 2010. "Dependency of the thermal and electrical conductivity on the temperature and composition of Cu in the Al based Al–Cu alloys". *Experimental Thermal and Fluid Science*, Vol. 34, No. 8, pp. 1507 – 1516. ISSN 0894-1777.

Aziz, M.J., 1982. "Model for solute redistribution during rapid solidification". *Journal of Applied Physics*, Vol. 53, No. 2, pp. 1158–1168.

Bhat, B.N., 1975. "Effect of thermotransport on directionally solidified aluminium-copper eutectic". *Journal of Crystal Growth*, Vol. 28, No. 1, pp. 68 – 76. ISSN 0022-0248.

Chen, S.W., Lin, C.C. and Chen, C., 1998. "Determination of the melting and solidification characteristics of solders using differential scanning calorimetry". *Metallurgical and Materials Transactions A*, Vol. 29, pp. 1965–1972.

Dantzig, J.A. and Rappaz, M., 2009. *Solidification*. EPFL press.

De Groot, S.R. and Mazur, P., 2013. *Non-Equilibrium Thermodynamics*. Dover Books on Physics. Dover Publications. ISBN 9780486153506.

Dobosz, A. and Gancarz, T., 2018. "Reference data for the density, viscosity, and surface tension of liquid Al–Zn, Ag–Sn, Bi–Sn, Cu–Sn, and Sn–Zn eutectic alloys". *Journal of Physical and Chemical Reference Data*, Vol. 47, No. 1, p. 013102.

Eslamian, M., Sabzi, F. and Saghir, M.Z., 2010. "Modeling of thermodiffusion in liquid metal alloys". *Physical Chemistry Chemical Physics*, Vol. 12, pp. 13835–13848.

Flemings, M.C., 1974. *Solidification processing*. Wiley Online Library.

Giordanengo, B., Benazzi, N., Vinckel, J., Gasser, J.G. and Roubi, L., 1999. "Thermal conductivity of liquid metals and metallic alloys". *Journal of Non-Crystalline Solids*, Vol. 250-252, pp. 377 – 383. ISSN 0022-3093.

Jafar-Salehi, E., Eslamian, M. and Saghir, M.Z., 2016. "Effect of thermodiffusion on the fluid flow, heat transfer, and solidification of molten metal alloys". *Engineering Science and Technology, an International Journal*, Vol. 19, No. 1, pp. 511–517.

Kurz, W. and Fisher, D.J., 1998. *Fundamentals of solidification*. Trans Tech Publications Ltd.

Platten, J.K. and Legros, J.C., 2012. *Convection in liquids*. Springer Science & Business Media.

Plevachuk, Y., Sklyarchuk, V., Yakymovych, A., Eckert, S., Willers, B. and Eigenfeld, K., 2008. "Density, viscosity, and electrical conductivity of hypoeutectic Al-Cu liquid alloys". *Metallurgical and Materials Transactions A*, Vol. 39, No. 12, pp. 3040–3045. ISSN 1543-1940.

Santos Filho, J.E. and Heringer, R., 2020. "Microsegregation model including Soret effect: an application for Sn-Bi alloy". In *Proceedings of MCWASP XV: Modelling of Casting, Welding and Advanced Solidification Processes. Accepted*.

Satheesh, A. and Mohan, C.G., 2017. "Computational investigation of double-diffusive mixed convective flow in an enclosed square cavity with Soret effect". *Frontiers in Heat and Mass Transfer (FHMT)*, Vol. 8.

Vizdal, J., Braga, M.H., Kroupa, A., Richter, K.W., Soares, D., Malheiros, L.F. and Ferreira, J., 2007. "Thermodynamic assessment of the Bi-Sn-Zn system". *CALPHAD: Comput. Coupling Phase Diagrams Thermochem.*, Vol. 31, pp. 438–448.

6. RESPONSIBILITY NOTICE

The author is solely responsible for the printed material included in this paper.